AIP Applied Physics Letters

Radial scale effect on the performance of low-power cylindrical Hall plasma thrusters

Mihui Seo, Jongsub Lee, Jongho Seon, Hae June Lee, and Wonho Choe

Citation: Applied Physics Letters **103**, 133501 (2013); doi: 10.1063/1.4820774
View online: http://dx.doi.org/10.1063/1.4820774
View Table of Contents: http://scitation.aip.org/content/aip/journal/apl/103/13?ver=pdfcov
Published by the AIP Publishing

Radial scale effect on the performance of low-power cylindrical Hall plasma thrusters

Mihui Seo,[1,a)] Jongsub Lee,[1,b)] Jongho Seon,[2] Hae June Lee,[3] and Wonho Choe[1,c)]
[1]*Department of Physics, Korea Advanced Institute of Science and Technology, 291 Daehak-ro, Yuseong-gu, Daejeon 305-701, Republic of Korea*
[2]*School of Space Research, Kyung Hee University, 1732 Deokyoungdaero, Giheung-gu, Yongin-si, Gyeonggi-do 446-701, Republic of Korea*
[3]*Department of Electrical Engineering, Pusan National University, Busandaehak-ro 63beon-gil, Geumjeong-gu, Busan 609-735, Republic of Korea*

(Received 15 June 2013; accepted 13 August 2013; published online 23 September 2013)

Investigation of the radial scale effect on low-power cylindrical Hall thrusters has been undertaken by comparing the thrusters with three different channel diameters of 28, 40, and 50 mm. The investigation found that both the anode efficiency and the thrust of the larger thruster are higher as the anode power is raised. On the other hand, higher current and propellant utilizations are achieved for the smaller thruster, which is due to higher neutral density and better electron confinement. The large plume angle of the small cylindrical Hall thruster causes thrust loss, resulting in the reduction of anode efficiency. © *2013 AIP Publishing LLC*. [http://dx.doi.org/10.1063/1.4820774]

Hall thrusters have recently gained much attention due to their advantages of a simple structure and power configuration that are suitable for advanced missions, especially for micro and small satellites.[1] Such applications of Hall thrusters generally require compact size, reduced mass and electric power below a few hundred watts. Therefore, a miniaturized discharge channel and large magnetic field are required in order to preserve sufficient ionization efficiency with a relatively low mass flow rate of Xe propellant.

Generally, the sub-kilowatt class low-power Hall thrusters are designed by scaling down of the well optimized, larger Hall thrusters.[2–4] Scaling laws for conventional annular thrusters (AHTs) have been studied[5–10] with respect to the mass flow rate and anode power, and applied to develop AHTs with various power levels. The small physical dimension of the conventional Hall thrusters, however, leads to difficulty in achieving an optimal magnetic field because of limited space for magnetic poles and/or heat shields.[11] Magnetic field configuration is closely related to particle loss, electron transport, heating, and erosion issues. Therefore, scaling down of thrusters usually brings about reduction of the overall thruster performance in terms of thrust, thrust efficiency, and lifetime.[12] It is known that 200 W class AHTs, such as BHT-200,[13] X-40,[14] SPT-30,[15] T-27,[16] operate in the anode efficiency range of 20% – 40%.

On the other hands, compared to the AHT, the cylindrical Hall thruster (CHT) having large volume-to-surface ratio due to removal of the inner section has been investigated as a means of improving the performance of compact Hall thrusters.[12,17–20] The cylindrical Hall thruster achieved anode efficiencies of about 20%–30% for anode power smaller than 200 W, but higher efficiency of 33%–41% has been obtained with "cathode overrunning" effect.[21] For CHTs, however, the difference in the magnetic field configuration from AHT due to the short inner core of CHT is known to result in quite different underlying physics in CHTs.[12,17–20] Thus, the design of CHT will deserve a separate investigation for better understanding and perhaps improvement of the performances. In this paper, we study the effects of channel size on CHTs from the viewpoint of performance optimization. Previously, the performance of CHTs in relation to channel[20] and the annular length[22] was investigated for low-power CHTs. In this study, the performance of three CHTs with different diameters is compared under various operation conditions to investigate the dependence on radial size at a similar input power level.

The CHTs under experiment consist of a boron nitride channel, a stainless steel anode that also serves as the Xe gas distributor, and a magnetic circuit as illustrated in Fig. 1. The magnetic circuit comprises inner and outer coils and an iron disk placed between the two coils. Experiments were carried out with three different thrusters having diameters (D) of 28 mm, 40 mm, and 50 mm, respectively. The channel length (L), defined as the distance between the anode and the thruster exit, was fixed at 24 mm, and the iron disk was placed at 10 mm from the thruster exit for all of the three thrusters. In the present study, the currents of the outer and inner coils were co-directed to produce an enhanced axial magnetic field and a stronger magnetic mirror effect. The magnetic field configuration was optimized to have the discharge stable with the minimized discharge current at the same Xe flow rate to compare the best performance for each thruster.

Figure 2(a) shows the calculated vacuum magnetic field lines in the discharge volume. As shown in Fig. 2(b), the magnetic field strength averaged over radius $|B|_{ave}$ at the optimized field configuration for each thruster is larger for a smaller thruster. In addition, although the maximum field strengths of the radial magnetic field B_r for each thruster are similar at the outer channel wall (340–350 G), the axial (B_z) and radial fields (B_r) are larger for a smaller thruster [Fig. 2(c)]. In these experiments, we find that a small thruster

[a)]Permanent address: Agency for Defense Development, Yuseong P.O.Box 35, Daejeon 305-600, Republic of Korea.
[b)]Permanent address: Samsung Electronics, 1 Samsungjeonja-ro, Hwasung-si, Gyeonggi-do 445-701, Republic of Korea.
[c)]Author to whom correspondence should be addressed. Electronic mail: wchoe@kaist.ac.kr.

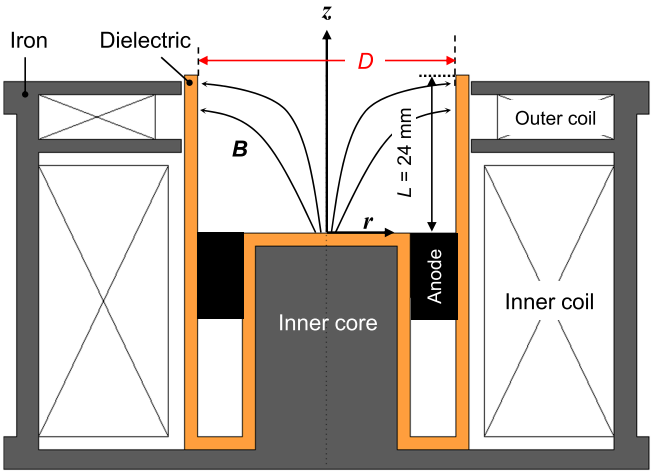

FIG. 1. A schematic illustration of the CHTs under experiment.

requires a strong magnetic field to operate under the optimized condition, which is related to electron confinement.

Through the experiments, the cathode keeper current and Xe flow rates were fixed at 1.6 A and 1 sccm, respectively. The 28, 40, 50 mm CHTs were operated at 3–6 sccm, 3–7 sccm, and 4–7 sccm Xe flow rates at the anode, respectively, at 225–350 V anode voltage. The experiments were performed inside a vacuum chamber of 3 m in length and 1.5 m in diameter, while the operating pressure was kept below 13 μTorr in the presence of continuous Xe flow. The thruster was mounted on a pendulum-type thrust balance, and the displacement of the thrust balance generated by plasma operation was measured by the combination of a laser and a position-sensitive diode detector. The ion energy distribution function (IEDF) and the plasma plume angle were measured by a retarding potential analyzer (RPA) and a Faraday probe, respectively. In this paper, we define θ_{90} and θ_{50} as plume angles that contain 90% and 50% of the total ion current, respectively, based on the angular ion beam current with respect to the thruster axis (z-axis in Fig. 1). Both the RPA and Faraday probe were mounted on a rotational motion stage with a radius of 37 cm centered at the thruster exit. Details of the measurement method of the probes are found elsewhere.[7]

The charge exchange collisional mean free path between the Xe^+ ion and background Xe neutral $\lambda_{i,n}^{cx}$ $(=v_i/(n_n\langle\sigma_{i,n}^{cx}v_i\rangle))$, where v_i, n_a, and $\sigma_{i,n}^{cx}$ (Ref. 23) are the ion speed, background neutral density, and charge exchange cross section between Xe^+ ion and neutral, respectively) at 13 μTorr operating pressure is 440 cm for 300 eV ions. On the other hand, the elastic collision mean free path $\lambda_{i,n}^{ec}$ $(=v_i/(n_n\langle\sigma_{i,n}^{ec}v_i\rangle))$, where $\sigma_{i,n}^{ec}$ (Refs. 24 and 25) is the Xe^+ ion and neutral elastic collision cross section) is 72 cm. Therefore, both the charge exchange reaction and elastic collision mean free paths are longer than the ion current measurement position from the thruster (37 cm).

As shown in Fig. 3, the three thrusters demonstrated similar tendencies under various discharge conditions. In

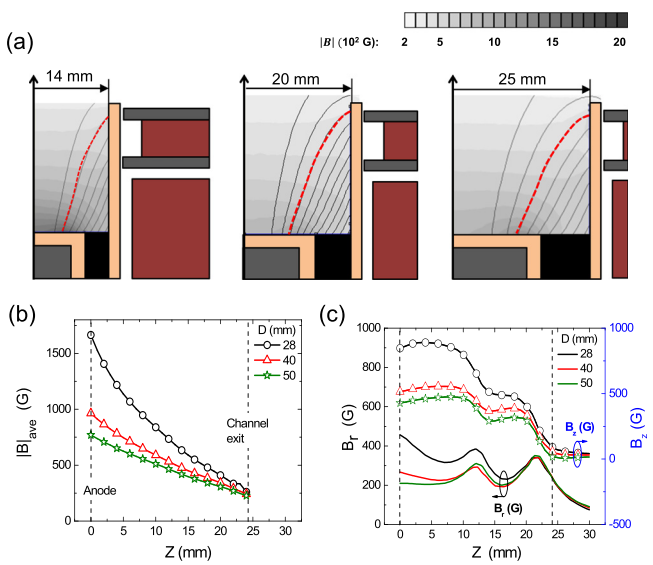

FIG. 2. (a) Magnetic fields of 28, 40, 50 mm thrusters, (b) average magnetic field strength along the thruster axis, (c) radial (solid curve), and axial (scattered curve) magnetic field strength along the outer channel surface.

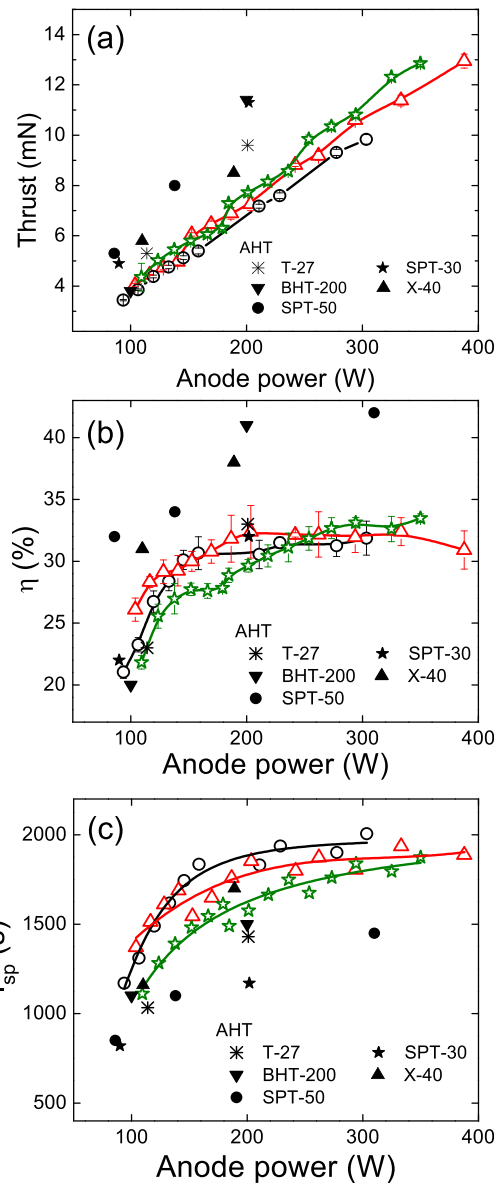

FIG. 3. (a) Thrust, (b) anode efficiency, and (c) specific impulse of 28 mm (○), 40 mm (△), and 50 mm (☆) CHT. Experimental results of some AHTs of the similar power level are also plotted for comparison.

order to compare with the radial effect of AHT, the parameters of low power AHTs (SPT-50,[26] BHT-200,[13] SPT X-40,[14] SPT-30,[15] T-27 (Ref. 16)) are also plotted in Fig. 3. Figure 3(a) shows the measured thrust T depending on the anode power P_a ($= I_d V_a$, where I_d and V_a are discharge current and anode voltage, respectively). It is seen that $T \propto P_a$, and the thrust increases slightly with increasing size of the thruster at the same P_a. The anode efficiency η ($=T^2/2\dot{m}I_d V_a$, where $\dot{m}$ is the Xe mass flow rate at the anode) shows an increase and then saturation as P_a is raised [Fig. 3(b)]. At $P_a > 250$ W, η of the 50 mm CHT is slightly higher than that of the other two smaller CHT. Although T and η of AHT are different from those of CHT, the tendencies are similar to the scaling down of AHT.[9] It is noteworthy that the scaling laws for CHT and AHT appear to be similar. However, the performance reduction of small AHT is caused by disadvantage of scaling down which mentioned before. Thus, as shown in Fig. 3(c), specific impulse I_{sp} ($=T/\dot{m}g$, where $g = 9.8$ m/s^2) of the small AHT is also lower. The lower I_{sp} means more propellant is needed to gain a given amount of momentum. For CHT, however, I_{sp} of smaller CHT is higher at the same P_a [Fig. 3(c)]. This distinguished feature will be explained more detail by comparing the utilizations.

To investigate the performance characteristics in more detail, the discharge current (I_d), ion current (I_i), electron current (I_e), and utilizations are compared at fixed $V_a = 300$ V. We obtain I_i by angular integration of the measured ion current density, and let $I_e = I_d - I_i$. Because the anode efficiency η of the larger thruster is higher at high P_a, η of the larger thruster is higher at larger $\dot{m}$. All the currents I_d, I_i, and I_e plotted in Figs. 4(a) and 4(b) increase linearly with $\dot{m}$. At the same $\dot{m}$, the larger thruster shows lower I_d, which may be attributed to lower neutral Xe density owing to larger discharge volume. It is also noted that I_i takes a larger fraction (or I_e takes a smaller fraction) in I_d for the smaller thruster. As a result, both current utilization $U_c[= I_i/(I_i + I_e)]$

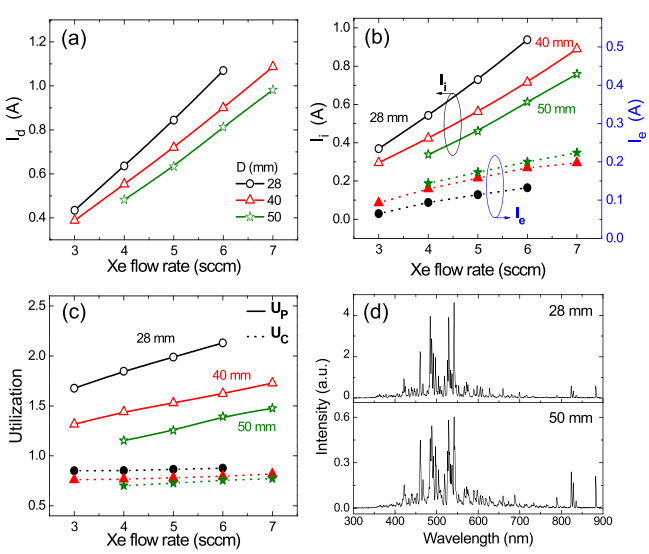

FIG. 4. (a) Discharge current, (b) ion and electron currents, (c) propellant utilization and current utilization in relation to D and $\dot{m}$. (d) Optical emission spectra of the 28 and 50 mm thrusters obtained at the radial center of the thruster exit plane at $P_a = 150$ W. An Ocean Optics USB2000 spectrometer was used.

and propellant utilization $U_p[=I_i M/e\dot{m}$, where M and e are the mass of a Xe atom and the electron charge, respectively] are larger for the smaller thruster [Figs. 4(b) and 4(c)]. The small I_e with a smaller thruster is interpreted as better electron confinement owing to the higher axial magnetic field and better magnetic mirror trapping. The largest magnetic mirror ratios are 4.9, 3.8, and 2.8 for the 28, 40, and 50 mm thrusters, respectively, according to the magnetic field line between the core and thruster exit plane (see scattered symbols in Fig. 2(a)).

Figure 4(c) indicates larger U_p at a higher Xe flow rate, which is due to more ionization by higher Xe neutral density. Larger U_p for smaller thrusters (the U_p ratio for the 28 mm and 40 mm thrusters with respect to the 50 mm thruster are 1.6 and 1.2, respectively) is attributed to the aforementioned reason, i.e., higher neutral density for a smaller thruster due to the smaller ionization volume. It is also noted that U_p is larger than the unity which has been previously reported and explained by the presence of multi-charged Xe ions in CHTs.[4–7] If the high neutral density with the same thruster only enhances ionization (or ionization rate), U_c should remain constant regardless of $\dot{m}$ because both I_i and I_e increase with the same rate. Figure 4(c), however, shows a slight increase of U_c with $\dot{m}$ for the same thruster. Therefore, we suggest the possible reason for the large U_p and U_c is the presence of multiply charged Xe ions. Enhanced multiply charged ion generation induces a higher increment rate of I_i than that of I_e due to the higher multiply charged ion speed in comparison with Xe^+, resulting in the larger U_p and U_c. Using the same logic, the large U_c of the small thruster is also interpreted in terms of the enhanced multiply charged ions as well as small I_e owing to better electron confinement. Furthermore, we suggest that the multiply charged ion have much effect on U_p and U_c than particle–wall interaction in the CHT.

The optical emission spectra of the 28 mm and 50 mm thrusters obtained at the radial center of the thruster exit plane are plotted in Fig. 4(d). Xenon plasma radiates emission spectra from collision processes among electrons, ions, and neutral atoms:[27] $Xe + e \rightarrow Xe^* + e$, $Xe^+ + Xe \rightarrow Xe^{+*} + Xe^*$, $Xe^{2+} + Xe \rightarrow Xe^{2+*} + Xe^* \rightarrow Xe^{+*} + Xe^{+*}$. As shown in the figure, the Xe neutral (Xe I) lines are dominant in the range of 750–900 nm and Xe^+ (Xe II) lines are dominant in the range of 400–600 nm. The intensity ratios of 529.22 nm (Xe II) and 823.16 nm (Xe I) of the 28 mm and 50 mm thrusters are 6.7 and 2.4, respectively. Upon even considering the much lower I_e for the smaller thruster despite its higher power density, the Xe II intensities are significantly higher, suggesting more active ionization in the smaller thruster.

Fig. 5(a) shows the peak values and the full width at half maximum (FWHM) of IEDF of the three thrusters. The peak ion energies are almost the same in the range of 220–240 eV, which suggests a similar electric potential structure for all the three thrusters. In addition, the FWHM of the 40 mm thruster increases as $\dot{m}$ is raised. Figure 5(b) plots the normalized IEDFs (i.e., $f(E)/\int f(E)dE$) of the 40 mm thruster measured at the thruster axis with various $\dot{m}$. It is observed that the thruster operation with higher $\dot{m}$ brings about broadening of the IEDF with an increase in high-energy

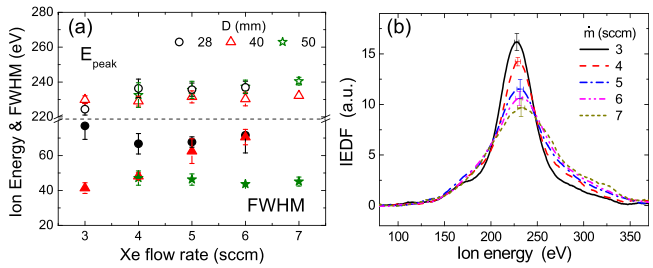

FIG. 5. (a) Peak ion energy and FWHM of IEDF in relation to D and $\dot{m}$, and (b) IEDFs of the 40 mm CHT with different $\dot{m}$.

population. Ions are accelerated by the potential difference lower than the anode voltage, i.e., $V_{acl} = V_a - V_{loss}$, where V_{loss} may include ionization potential, wall loss, cathode coupling potential, etc. Nevertheless, more ions with energy higher than V_a (300 V in this case) are generated as $\dot{m}$ increases. Previous reports[28,29] have discussed the high-energy tail of the IEDF due to elastic momentum transfer collisions between Xe^+ and Xe^{2+} in the plume plasma: momentum gained Xe^+ from the high-energy Xe^{2+} that are generated in the discharge volume. Therefore, the increase of the high-energy population with large $\dot{m}$ is interpreted as enhanced collision probability between Xe^+ and high energy Xe^{2+} ions by more generated multi-charged ions. Although the increased high-energy population in the IEDF with $\dot{m}$ is also observed in the 50 mm thruster, the difference is smaller than that of the 40 mm thruster. We suggest that the large discharge volume reduces the fractional increment of the neutral density and thus, generation of Xe^{2+}. On the other hand, the IEDF of the 28 mm thruster is little changed with different $\dot{m}$. As shown in Fig. 4(c), the propellant utilization U_p of the 28 mm thruster is nearly 2, which suggests a large population of multi-charged ion generation. Detailed study of the multi-charged ions and high-energy fraction based on the E × B filter and RPA measurements will be reported elsewhere.

In Fig. 6(a), the IEDF broadening, i.e., spread of the ion energy spectrum is shown for various channel sizes at $\dot{m} = 4$ sccm and $V_a = 300$ V. The fraction of the high-energy ion population is more significant for the smaller thruster, which is similar to the higher $\dot{m}$ case shown in Fig. 5(b). Therefore, high neutral density owing not only to the increased $\dot{m}$ but also to the decreased channel size may have a close correlation with high-energy ion production or multi-charge ion population.

The plume angle obtained from the angular profile of the ion current density depicted in Fig. 6(b) is smaller for the larger thruster and at smaller $\dot{m}$. This can be explained by the fact that the different channel diameter with the fixed channel length can change the slope of the magnetic field line as shown in red dotted curves in Fig. 2(a). It was reported that the unique magnetic field configuration of the CHT with a relatively strong axial component [Fig. 2(c)] generates an electric field normal to the magnetic field.[2,3] Therefore, the large diameter-to-length ratio of the large thruster brings about the small plume angle. As shown in Fig. 2(a), the angles of the red colored magnetic field lines connected from the inner core to the exit side of the discharge volume with respect to the anode surface are 66.6°, 58.4°, and 54.0° for the 28, 40, 50 mm thrusters, respectively. Theses angles are comparable with θ_{90} shown in Fig. 6(b). Also, the neutral

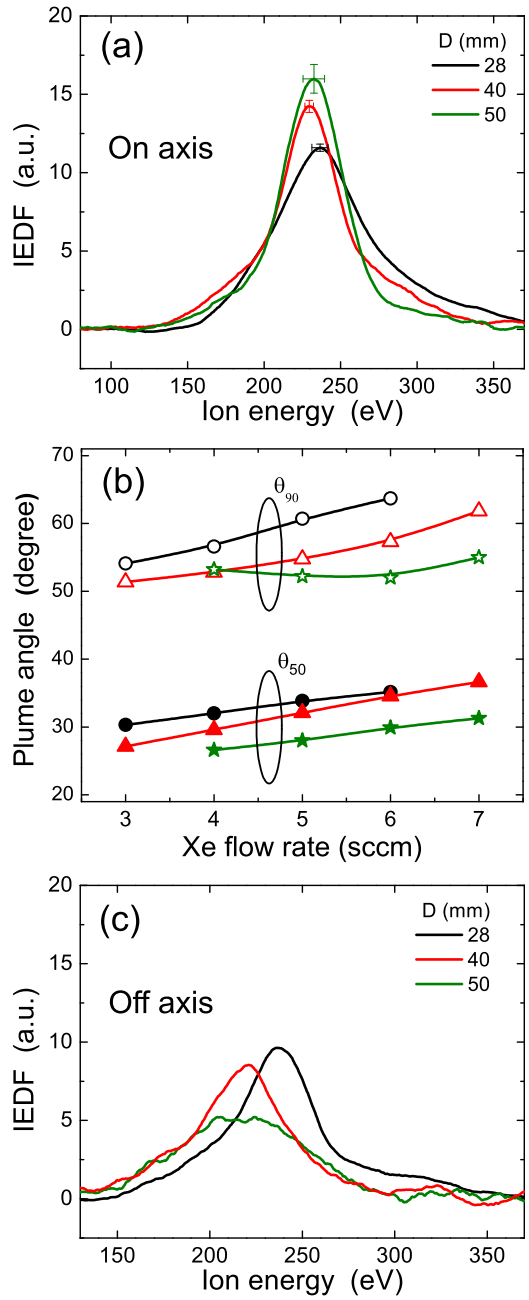

FIG. 6. (a) IEDFs at thruster axis and (b) 30° off-axis with various D values at 4 sccm, and (c) plume angles θ_{90} and θ_{50} in relation to D and $\dot{m}$.

density associated with the channel dimension may play a role in the plume angle difference.

As for the ion energy spectrum, results were obtained by comparing the IEDFs measured on-axis [Fig. 6(a)] and 30° from the thruster axis [Fig. 6(c)] with the radius of 37 cm from the thruster exit. First, the larger drop of the peak value from the 0° IEDF to the 30° IEDF demonstrates the smaller plume angle for the larger thruster. Second, the ion energy drop off-axis is more significant for the larger thruster that is seen from the larger down shift of the energy peak. Third, in the 28 mm thruster the peak value and its energy are almost the same for 0° and 30°, meaning that the ion current density is more or less uniform up to 30°. On the other hand, θ_{50} shown in Fig. 6(b) indicates a drop in the ion current density between 30° and 50°. It is also noteworthy that the high-energy ion population mostly decreases at 30° for the 28 mm

thruster. Because the thrust loss ($\sim\cos\theta_{90}$) is associated with plume divergence, spatial focusing of the ion beam is important for high performance of the thruster.[30,31] Therefore, smaller plume divergence and higher propellant and current utilizations of the 50 mm thruster with larger $\dot{m}$ enhance the power efficiency.

On the other hand, shorter channel length of 28 mm may focus the ion beam and reduce the thrust loss, resulting in the anode efficiency improvement. However, the short channel length yields the reduced propellant utilization and ion energy.[20] Therefore, optimization of channel length is a critical process.

As mentioned above, the high-energy ion population at 30° off-axis is lower than that on-axis. Because the elastic collision between Xe^{+} and Xe^{2+} produces the high-energy tail of IEDF,[28,29] it is likely that the multi-charged ions inside the discharge volume are concentrated near the thruster axis and are responsible for the large high-energy ion population on-axis. This argument is consistent with Ref. 32, which explains the multi-charged ions of CHT by the long residence time of the slow ions due to their ambipolar trapping near the thruster axis.

In summary, the performance of the low-power cylindrical Hall thruster in relation to channel diameter was investigated. Comparisons with annular type Hall thruster find that the overall scaling property for the reduction of thruster size appear to be similar, but this study clearly demonstrates that different physics needs to be accounted for the cylindrical Hall thrusters. It was found that the high neutral density due to the small channel size and high mass flow rate enhance the propellant utilization and current utilization by increased ion current. Also, the high ion energy population of IEDF increases with high neutral density. As a result, the smaller thruster and large mass flow rate produce high specific impulse. However, the thrust and anode efficiency of the smaller thruster is lower at the anode power above 150 W because of the large plume angle due to the large magnetic field line slope with respect to the anode surface. On the other hand, the narrow plume of the large thruster is maintained in relation to $\dot{m}$ and anode power. This effect combines with the advantage of high neutral density and enhances the thrust and thrust efficiency at high anode power (>250 W).

The authors thank Mr. Seongmin Kang of Satrec Initiative for the 50 mm thruster. This work was supported by the National Space Laboratory (NSL) (Grant No. 2012-00009098) through the National Research Foundation of Korea funded by the Ministry of Education, Science and Technology.

[1]J. Mueller, C. Marrese, J. Ziemer, A. Green, E. H. Yang, M. Mojarradi, T. Johnson, V. White, D. Bame, R. Wirz, M. Tajmar, V. Hruby, M. Gamero-Castaño, J. Schein, and R. Reinicke, in Nanotech 2002, Houston, USA, AIAA Paper No. 2002-5714, 2002.
[2]A. V. Loyan, N. N. Koshelev, T. A. Maksymenko, A. Leufroy, S. Pellerin, T. Gibert, N. Pellerin, E. Veron, D. Pagnon, L. Balika, and M. Dudeck, Rom. J. Phys. **56**(Supplement), 95 (2011).
[3]B. E. Beal and A. D. Gallimore, Phys. Plasmas **12**, 123503 (2005).
[4]N. Z. Warner, Ph.D. dissertation, Massachusetts Institute of Technology, 2007.
[5]V. Khayms, M.S. dissertation, Massachusetts Institute of Technology, 1997.
[6]V. Kim, V. Kozlov, A. Kazurenko, G. Popov, A. Skrylnikov, C. Clauss, M. Day, and J. Sankovic, in 34th Joint Propulsion Conference, Cleveland, USA, AIAA Paper No. 98-3335, 1998.
[7]F. Battista, E. De Marco, T. Misuri, and M. Andrenucci, in 30th International Electric Propulsion Conference, Florence, Italy, Paper No. IEPC–2007–313, 2007.
[8]Y. J. Ding, D. R. Yu, D. C. Kia, G. J. Yan, and H. Li, Contrib. Plasma Phys. **51**, 68 (2011).
[9]E. Ahedo and J. M. Gallardo, in 28th International Electric Propulsion Conference, Toulouse, France, Paper No. IEPC-2003–104, 2003.
[10]M. Andrenucci, L. Biagioni, S. Marcuccio, and F. Paganucci, in 28th International Electric Propulsion Conference, Toulouse, France, Paper No. IEPC-2003-259, 2003.
[11]A. Simirnov, Y. Raitses, and N. J. Fisch, J. Appl. Phys. **92**, 5673 (2002).
[12]Y. Raitses and N. J. Fisch, Phys. Plasmas **8**, 2579 (2001).
[13]V. Hruby, J. Monheiser, B. Pote, P. Rosler, J. Kolencik, and C. Freeman, in 30th Plasmadynamics and Lasers Conference, Norfolk, USA, AIAA Paper No. 99-3534, 1999.
[14]M. B. Belikov, O. A. Gorshkov, A. B. Jakupov, and S. A. Khartov, in 34th Joint Propulsion Conference, Cleverland, USA, AIAA Paper No. 98-3786, 1998.
[15]D. T. Jacobson and R. S. Jankovsky, in 34th Joint Propulsion Conference, Cleverland, USA, AIAA Paper No. 98-3792, 1998.
[16]L. Zakharenkov, G. Chislov, A. Semenkin, and T. Lawrence, in 27th International Electric Propulsion Conference, Pasadena, USA, Paper No. IEPC-01-041, 2001.
[17]A. Smirnov, Y. Raitses, and N. J. Fisch, J. Appl. Phys. **94**, 852 (2003).
[18]A. Smirnov, Y. Raitses, and N. J. Fisch, Phys. Plasmas **14**, 057106 (2007).
[19]A. Smirnov, Y. Raitses, and N. J. Fisch, J. Appl. Phys. **95**, 2283 (2004).
[20]J. Lee, M. Seo, J. Seon, H. J. Lee, and W. Choe, Appl. Phys. Lett. **99**, 131505 (2011).
[21]Y. Raitses, A. Smirnov, and N. Fisch, Appl. Phys. Lett. **90**, 221502 (2007).
[22]M. Seo, J. Lee, J. Seon, H. J. Lee, and W. Choe, Phys. Plasmas **20**, 023507 (2013).
[23]J. S. Miller, S. H. Pullins, D. J. Levandier, Y. H. Chiu, and R. A. Dressler, J. Appl. Phys. **91**, 984 (2002).
[24]See supplementary material at http://dx.doi.org/10.1063/1.4820774 for the analytical total cross section versus center-of-mass energy for calculating the elastic collision mean free path; or A. V. Phelps (Unpublished), ftp://jila.colorado.edu/~avp/collision_data/ionneutral/ionatom.txt.
[25]A. V. Phelps, J. Appl. Phys. **76**, 747 (1994).
[26]D. H. Manzella, S. Oleson, J. Sankovic, T. Haag, A. Semenkin, and V. Kim, in 32nd AIAA/ASME/SAE/ASEE Joint Propulsion Conference, Vista, USA, AIAA Paper No. 96-2736, 1996.
[27]Y. Chiu, B. L. Austin, S. Williams, G. F. Karabadxhak, and R. A. Dressler, J. Appl. Phys. **99**, 113304 (2006).
[28]L. B. King, Ph. D. dissertation, University of Michigan, 1998.
[29]L. B. King and A. D. Gallimore, J. Propul. Power **16**, 916 (2000).
[30]Z. Ning, H. Liu, D. Yu, and Z. Zhou, Appl. Phys. Lett. **99**, 221502 (2011).
[31]C. W. Larson, D. L. Brown, and W. A. Hargus, in 43rd AIAA/ASME/SAE/ASEE Joint Propulsion Conference and Exhibit, Cincinnati, USA, AIAA Paper No. 2007-5270, 2007.
[32]A. Smirnov, Y. Raitses, and N. J. Fisch, in 40th AIAA/ASME/SAE/ASEE Joint Propulsion Conference and Exhibit, Florida, USA, AIAA Paper No. 2004-4103, 2004.